J Mater Sci (2016) 51:3564–3573
DOI 10.1007/s10853-015-9676-7

The effect of nanostructure on the tensile modulus of carbon fibers

Yunjiao Zhong[1] · Wenfeng Bian[1] · Meiling Wang[1]

Received: 28 June 2015 / Accepted: 15 December 2015 / Published online: 28 December 2015
© Springer Science+Business Media New York 2015

Abstract Using the Eshelby equivalent inclusion theory and the Mori–Tanaka method, a new micromechanical model is proposed to predict the tensile modulus of carbon fibers by considering crystallites, amorphous components, and microvoids of the fiber structure. Factors that affect the tensile modulus included the aspect ratio of crystallites, the aspect ratio of microvoids, the volume fraction of crystallites, the volume fraction of microvoids, and the orientation degree of crystallites. To follow the dependence of the tensile modulus of the fibers on microstructure, thirty different types of polyacrylonitrile-based fibers were prepared. The aspect ratios and orientation degrees of crystallites were calculated directly by X-ray diffraction. The aspect ratios and volume fractions of microvoids were obtained by small-angle X-ray scattering. The average tensile modulus of amorphous was estimated by dealing with thirty types of PAN-based fibers. The volume fractions of crystallites were obtained by the micromechanical model. Some relationships are concluded: (1) the tensile modulus increased with increasing volume fractions of crystallites, aspect ratios of crystallites and microvoids, and orientation degree of crystallites; (2) the tensile modulus increased with decreasing volume fractions of microvoids.

✉ Yunjiao Zhong
zhongyunjiao@126.com

[1] Department of Astronautic Science and Mechanics, Harbin Institute of Technology, Harbin 150001, China

Introduction

Carbon fibers have high specific tensile modulus and strength, and play an important role in civil engineering construction, aerospace field, automotive materials, athletic equipment, etc. To improve the properties of carbon fibers, many studies have been undertaken to see the relationships between the mechanical properties and structure. The structure and morphology of carbon fibers have been studied by Oberlin [1], Johnson [2, 3], and Donnet [4]. Various mechanical models were introduced. The uniform stress mechanical model and the mosaic model of carbon fibers, both consisting of aligned crystallites connected with each other, were introduced to explain quantitatively the association between the tensile modulus and the crystallite orientation. The uniform stress mechanical model is able to describe the behavior of graphitized carbon fibers and shows the significance of the axial shear modulus on the bulk carbon fibers tensile modulus [5, 6]. The mosaic mechanical model can explain the measured increases in the tensile modulus and the crystallite orientation dependence on tensile stress [7]. Because the carbon fiber has a unique microstructure which consists of carbon crystallite layers, crystallite disorder regions (amorphous phase), and needle-like microvoids [8], a series–parallel mechanical model which comprises crystalline and amorphous phase is introduced. This series–parallel model can evaluate the heterogeneous stress distribution in the carbon fibers [9]. More recently, a two-phase composite micromechanical model which took into account the properties of both the crystalline and the amorphous components in the fiber structure was established to predict the tensile modulus of polyacrylonitrile (PAN)-based carbon fibers [10].

However, the uniform stress mechanical model and the mosaic model are unable to predict the behavior of low

modulus PAN-based carbon fibers because they are too simplified and ignore the disordered structure. All models [5–7, 9, 10] mentioned above paid no attention to the microvoids whose content was about 10–20 volume percent in carbon fibers [11]. We think that there must be a connection between the volume percent of microvoids and mechanical properties of the carbon fibers. In this study, we introduce a new three-phase composite micromechanical model to predict the tensile modulus of PAN-based carbon fibers by considering the crystallites, the amorphous components, and the microvoids in the fiber structure. The combination of Eshelby's solution [12, 13] and Mori–Tanaka's mean stress method [14] is used to calculate the elastic coefficients. The X-ray diffraction (XRD) and small-angle X-ray scattering (SAXS) methods are applied to measure the experimental data of crystallites and microvoids in carbon fibers. Some factors that have an influence on tensile modulus of carbon fibers upon the microstructure are discussed.

Theoretical model

In this section, we establish the micromechanical model that is composed of crystallites, amorphous components, and microvoids to predict the tensile modulus of the carbon fibers. The amorphous components are assumed to be an isotropic matrix. The crystallites and the microvoids are regarded as inclusions in the isotropic matrix.

The true shape of crystallites and the microvoids are particularly complex in carbon fibers. However, it is reasonable that the shape of the crystallites is equivalent to oblate spheroids with the carbon layer axis parallel to their long axes. Moreover, the shape of the microvoids is equivalent to a long rotational ellipsoid [8, 10]. See Fig. 1. The concept of representative volume element (RVE) V in the carbon fibers is introduced. We assume that the RVE is subjected to remote boundary conditions, e.g., see Ref. [15, 16]. We also assume that (1) the amorphous carbon has a Poisson's ratio of 0.3 [10]; (2) the coefficients of the elastic tensor of the crystallites are the same as those of graphite [17]; (3) the shape of the crystallites is an oblate spheroid, and the aspect ratio of the oblate spheroid ω_c is given by $\omega_c = L_a/L_c$,where L_a is the crystallite diameter and L_c is the crystallite thickness, both of them are measured by XRD; (4) the shape of the microvoids is a rotation ellipsoid, and the aspect ratio of the rotation spheroid ω_v is given by $\omega_v = L/a$, where L is the half length of rotation axis of the microvoid and a is the radius length, both of them are determined by SAXS; (5) the total volume fraction of crystallite, amorphous carbon, and microvoid is equal to unity.

A global coordinate system $O{-}x_1x_2x_3$ is established in carbon fibers to ensure that the axis $x_3$coincides with the fiber axis. Two local coordinate systems $O - x_1'x_2'x_3'$ and $O - x_1''x_2''x_3''$ in the crystallite and microvoid are also established, respectively. Let the axis x_3' coincide with the rotation axis of crystallite and the x_3'' coincide with the microvoid rotation axis.

The carbon fiber is subjected to a uniform applied stress σ_0, by Eshelby equivalent inclusion theory [17], we derive that the relation within the crystallite $(O - x_1'x_2'x_3')$ is described by

$$C_0\left(\varepsilon^{0'} + \tilde{\varepsilon}' + S_1\varepsilon^{*'} - \varepsilon^{*'}\right) = C_1\left(\varepsilon^{0'} + \tilde{\varepsilon}' + S_1\varepsilon^{*'}\right), \qquad (1)$$

where C_0 and C_1 are the elastic coefficients of the amorphous carbon and the crystallite carbon in the fibers, S_1 is the fourth-order Eshelby tensor of the crystallite inclusion which has an oblate spheroid shape, e.g., see S_1 in [18]. $\varepsilon^{0'}$ is the strain in the isotropic matrix having no crystallites and microvoids, $\tilde{\varepsilon}'$ is the average perturbed strain that

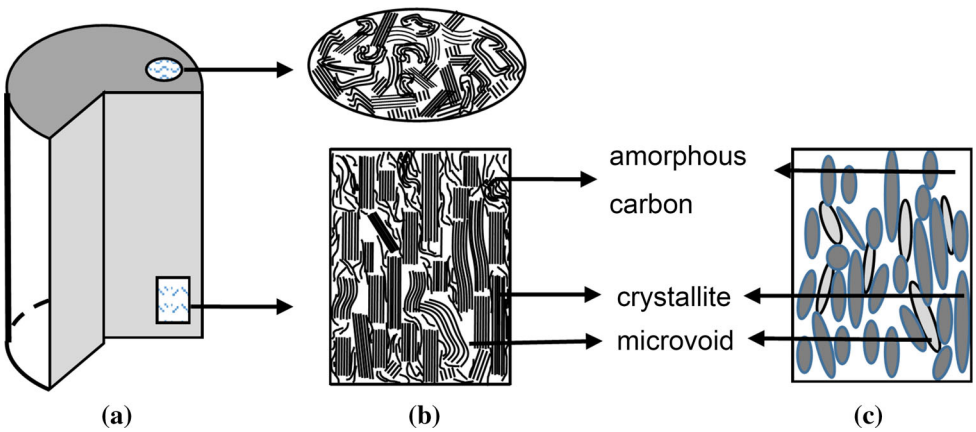

Fig. 1 **a** model of the carbon fiber, **b** the structure of (**a**), (**c**) the modeling of (**b**)

caused by interactions between crystallites and microvoids, $\varepsilon^{*'}$ is the equivalent eigenstrain of the crystallite.

Similarly, we can derive that the relation in the microvoid $(O - x_1''x_2''x_3'')$. The mentioned relation is

$$C_0\left(\varepsilon^{0''} + \tilde{\varepsilon}'' + S_2\varepsilon^{**''} - \varepsilon^{**''}\right) = 0, \tag{2}$$

where S_2 is the fourth-order Eshelby tensor of the microvoid inclusion which has a rotational ellipsoid shape, e.g., see S_2 in [19], $\varepsilon^{0''}$ is the strain in the isotropic matrix having no crystallites and microvoids, $\tilde{\varepsilon}''$ is the average perturbed strain that caused by interactions between crystallites and microvoids, and $\varepsilon^{**''}$ is the equivalent eigenstrain of the microvoid.

From (1) and (2), we obtain the equivalent eigenstrain of the crystallite ε^{*} and the equivalent eigenstrain of the microvoid ε^{**} in the carbon fiber $(O - x_1'x_2'x_3')$ by coordinate transformation. The expressions for ε^{*} and ε^{**} are

$$\varepsilon^{*} = -\left(T_1^{-1}\right)^{\mathrm{T}}(\Delta\mathrm{CS}_1 + C_0)^{-1}\Delta\mathrm{C}T_1^{\mathrm{T}}\left(\varepsilon^{0} + \tilde{\varepsilon}\right), \tag{3}$$

$$\varepsilon^{**} = -\left(T_2^{-1}\right)^{\mathrm{T}}(S_2 - I)^{-1}T_2^{\mathrm{T}}\left(\varepsilon^{0} + \tilde{\varepsilon}\right), \tag{4}$$

where $\Delta C = C_1 - C_0$, I is the unit matrix, T_1 and T_2 are transformation matrices between the two local coordinate systems and the global coordinate system, respectively. See T_1 and T_2 in the appendix. ε^0 is the strain in the isotropic matrix having no crystallites and microvoids, $\tilde{\varepsilon}$ is the average perturbed strain that caused by interactions between crystallites and microvoids.

We let $\langle\varepsilon\rangle_1$ and $\langle\varepsilon\rangle_2$ be the average strains in a crystallite and a microvoid, and we obtain

$$\langle\varepsilon\rangle_1 = \varepsilon^0 + \tilde{\varepsilon} + \varepsilon^1, \quad \langle\varepsilon\rangle_2 = \varepsilon^0 + \tilde{\varepsilon} + \varepsilon^2 \tag{5}$$

where $\varepsilon^1 = \left(T_1^{-1}\right)^{\mathrm{T}}S_1T_1^{\mathrm{T}}\varepsilon^{*}$ and $\varepsilon^2 = \left(T_2^{-1}\right)^{\mathrm{T}}S_2T_2^{\mathrm{T}}\varepsilon^{**}$ are the perturbed strains by the crystallite and the microvoid. Substituting (3) and (4) into (5) and let $\varepsilon^0 + \tilde{\varepsilon} = \langle\varepsilon\rangle_M$, we have

$$\langle\varepsilon\rangle_1 = \left[I - \left(T_1^{-1}\right)^{\mathrm{T}}S_1(\Delta\mathrm{CS}_1 + C_0)^{-1}\Delta\mathrm{C}T_1^{\mathrm{T}}\right]\langle\varepsilon\rangle_M, \tag{6}$$

$$\langle\varepsilon\rangle_2 = \left[I - \left(T_2^{-1}\right)^{\mathrm{T}}S_2(S_2 + I)^{-1}T_2^{\mathrm{T}}\right]\langle\varepsilon\rangle_M, \tag{7}$$

Based on Mori–Tanaka method, we derive that the average strain field $\langle\varepsilon\rangle_V$ in V as follows:

$$\langle\varepsilon\rangle_V = \frac{1}{V}\int_{V-V_1-V_2}\langle\varepsilon\rangle_M\mathrm{d}V + \frac{1}{V}\int_{V_1}\langle\varepsilon\rangle_1\mathrm{d}V + \frac{1}{V}\int_{V_2}\langle\varepsilon\rangle_2\mathrm{d}V, \tag{8}$$

where V_1 is the sum of the volume of all crystallites in V, and V_2 is the sum of the volume of all microvoids in V.

Substituting (6) and (7) into (8), and considering orientation distribution of crystallites and microvoids, we have

$$\langle\varepsilon\rangle_V = \left[I - f_1\left\{\left(T_1^{-1}\right)A^1T_1^{\mathrm{T}}\right\}_{1\,\mathrm{angle}} - f_2\left\{\left(T_2^{-1}\right)^{\mathrm{T}}A^2T_2^{\mathrm{T}}\right\}_{2\,\mathrm{angle}}\right]\langle\varepsilon\rangle_M, \tag{9}$$

where $A^1 = S_1(\Delta\mathrm{CS}_1 + C_0)^{-1}\Delta C$, $A^2 = S_2(S_2 - I)^{-1}$, f_1 and f_2 are the volume fractions of the crystallites and the microvoids, $f_0 = 1 - f_1 - f_2$ is the volume fraction of amorphous, $\{\bullet\}_{i\,angle} = \int_0^{2\pi}\int_0^{\pi}\bullet\eta_i(\theta)sin\theta\mathrm{d}\theta\mathrm{d}\varphi/2\pi\int_0^{\pi}\eta_i(\theta)\sin\theta\mathrm{d}\theta$, $i = 1, 2$, and $\eta_1(\theta)$ and $\eta_2(\theta)$ are the distribution densities of the crystallites and microvoids, respectively.

Similarly, the average stress field $\langle\sigma\rangle_V$ in the carbon fiber can be derived as

$$\langle\sigma\rangle_V = \frac{1}{V}\int_{V-V_1-V_2}\langle\sigma\rangle_M\mathrm{d}V + \frac{1}{V}\int_{V_1}\langle\sigma\rangle_1\mathrm{d}V, \tag{10}$$

where $\langle\sigma\rangle_1$ is the average stress of a crystallite, and $\langle\sigma\rangle_M$ is the average stress of amorphous. The expressions are

$$\langle\sigma\rangle_1 = T_1C_1T_1^{\mathrm{T}}(\varepsilon^0 + \tilde{\varepsilon} + \varepsilon^1) = T_1C_1T_1^{\mathrm{T}}\langle\varepsilon\rangle_1, \tag{11}$$

$$\langle\sigma\rangle_M = T_1C_0T_1^{\mathrm{T}}(\varepsilon^0 + \tilde{\varepsilon}) = T_1C_0T_1^{\mathrm{T}}\langle\varepsilon\rangle_M = C_0\langle\varepsilon\rangle_M. \tag{12}$$

So

$$\langle\sigma\rangle_V = \frac{1}{V}\int_{V-V_1-V_2}C_0\langle\varepsilon\rangle_M\mathrm{d}V + \frac{1}{V}\int_{V_1}T_1C_1T_1^{\mathrm{T}}\langle\varepsilon\rangle_1\mathrm{d}V \tag{13}$$

by substituting (11) and (12) into (10) yields

Substituting (6) into (13), then

$$\begin{aligned}\langle\sigma\rangle_V &= [f_0C_0 + f_1\{T_1C_1[I - S_1(\Delta\mathrm{CS}_1 + C_0)^{-1}\Delta C]T_1^{\mathrm{T}}\}_{1\,angle}]\langle\varepsilon\rangle_M \\ &= \left[f_0C_0 + f_1\left\{T_1C_1\left[I - A^1\right]T_1^{\mathrm{T}}\right\}_{1\,angle}\right]\langle\varepsilon\rangle_M\end{aligned} \tag{14}$$

Note that $\langle\sigma\rangle_V = \bar{C}\langle\varepsilon\rangle_V$, we have

$$\bar{C} = \left[f_0C_0 + f_1\left\{T_1C_1\left[I - A^1\right]T_1^{\mathrm{T}}\right\}_{1\,angle}\right] \cdot \left[I - f_1\left\{\left(T_1^{-1}\right)^{\mathrm{T}}A^1T_1^{\mathrm{T}}\right\}_{1\,angle} - f_2\left\{\left(T_2^{-1}\right)^{\mathrm{T}}A^2T_2^{\mathrm{T}}\right\}_{2\,angle}\right] \tag{15}$$

Experimental

Materials

In order to research the dependence of the mechanical properties of the carbon fibers on nanostructure, we prepared thirty different types of PAN-based carbon fibers, with Young's moduli in the range 200–500 GPa. All experimental fibers were supplied by tuozhan fiber Co., Ltd and were measured by XRD and SAXS. Their properties are listed in Table 1.

XRD measurements

The XRD experiment was performed at National Laboratory of tuozhan fiber Co., Ltd. Weihai, China using CuKα radiation ($\lambda = 0.1541$ nm) under the operating conditions of 40 kV and 40 mA. We carried out axial scan, radial scan, and azimuth angle scan with 2θ-scan step 0.02° and 0.504°, respectively.

SAXS measurements

SAXS measurement was carried out at the beam line (BL16B1) of the Shanghai synchrotron radiation facility with a wavelength of 0.124 nm. The distance from sample to the detector was 5120 mm.

Results and discussion

XRD

L_c and L_a can be obtained from (002) diffraction peak of axial scan profile and (100) diffraction peak of radial scan profile using Scherrer's formula

Table 1 Physical and mechanical properties of the carbon fibers

Type	Tensile modulus (GPa)	Density (g/cm^3)	L_c (nm)	L_a (nm)	ω_c	d_{002} (nm)	H (°)	X_c (%)	f_2 (%)	Π (%)
TC35-3K	223.58	1.80	1.58	–	–	0.3479	–	–	7.52	–
UMS40-12K	380.00	1.79	3.66	–	–	0.3442	–	–	11.24	–
T700-12K	230.56	1.80	1.93	4.19	2.18	0.3543	37.03	71.77	9.46	79.43
HTS40-12K	239.04	1.76	1.91	–	–	0.3561	–	–	10.98	–
M46JB-12K	391.96	1.84	4.34	–	–	0.3426	–	–	10.41	–
TC36S-12K	237.97	1.81	1.68	–	–	0.3552	–	–	9.75	–
M35JB-6K	301.07	1.75	3.11	–	–	0.3482	–	–	12.94	–
A42-12K	240.00	1.80	1.85	–	–	0.3552	–	–	9.97	–
TC35-24K	210.62	1.76	1.56	–	–	0.3573	–	–	9.23	–
M40JB-6K	349.80	1.75	3.76	–	–	0.3430	–	–	11.66	–
STS40-24K	219.72	1.76	1.73	–	–	0.3564	–	–	9.84	–
TC42S-12K	231.52	1.81	1.98	–	–	0.3540	–	–	10.69	–
UM40-24K	355.59	1.79	3.43	–	–	0.3451	–	–	11.46	–
CCF300-3K	213.69	1.76	1.86	–	–	0.3558	–	–	12.08	–
CCF700-12K	234.66	1.79	1.86	–	–	0.3537	–	–	10.70	–
T300-3K	211.05	1.76	1.69	3.73	2.21	0.3558	36.26	68.36	9.73	79.68
T800HB-6K	278.30	1.81	2.10	–	–	0.3517	–	–	9.28	–
M40JB-12K	351.67	1.75	3.58	10.27	2.87	0.3443	22.14	81.49	11.87	87.70
TR50S-6K	240.01	1.82	1.89	–	–	0.3532	–	–	10.45	–
HS40-12K	388.29	1.85	4.44	–	–	0.3428	–	–	13.56	–
M35JB-12K	320.76	1.75	3.00	9.47	3.16	0.3456	24.72	79.20	12.61	86.27
SGL50K	215.80	1.79	1.65	–	–	0.3550	–	–	10.83	–
TC36-3K	206.55	1.81	2.04	–	–	0.3493	–	–	9.76	–
A49-12K	238.86	1.79	2.17	–	–	0.3504	–	–	12.60	–
HTA40-1K	240.85	1.78	2.12	–	–	0.3481	–	–	10.53	–
HTA-W3K	236.50	1.76	1.92	–	–	0.3566	–	–	10.02	–
TC35-12K	230.71	1.80	1.72	–	–	0.3576	–	–	9.09	–
TC35-48K	216.71	1.81	1.83	–	–	0.3545	–	–	10.75	–
TC33-3K	237.55	1.80	1.76	–	–	0.3556	–	–	10.64	–
T800H-12K	283.75	1.81	1.98	4.62	2.33	0.3543	28.77	72.94	8.92	84.02

$$L = K\lambda/B\cos\theta, \tag{16}$$

where θ is the scattering angle, λ is the wavelength of the X-rays used, and B is the full width at half maximum (FWHM) of diffraction peak. The form factor K is 0.9 for L_c and 1.84 for L_a [20]. The FWHM of an azimuthal scan through the (002) reflection H can be directly obtained from azimuth angle scan profile. The value of the average interlayer spacing d_{002} can be calculated using Bragg's law

$$d_{002} = n\lambda/2\sin\theta, \tag{17}$$

where n is an integer. The apparent crystallinity of the carbon fiber X_c is given by [21]

$$X_c = S_c/S_t \times 100\,\%, \tag{18}$$

where S_c is the area of (002) diffraction Peak and S_t is the total area under the diffraction curve in the interval [14°, 34°]. The degree of crystallites orientation Π can be calculated applying the formula

$$\Pi = (180^\circ - H)/180^\circ \times 100\,\%. \tag{19}$$

Detailed data are presented in Table 1.

Thirty different types of experimental carbon fibers were prepared to obtain the tensile modulus of amorphous, see Table 1. Figure 2 shows the bulk tensile modulus E_{bulk} versus their crystallite thickness L_c. The tensile modulus of fibers that are composed of amorphous carbon and microvoids $E_{a+m} = 111.48$ GPa. This value was obtained by extrapolating the straight linear line (linear regression) of E_{bulk} versus L_c to zero position [9]. To simplify the calculations, let the shape of microvoids in the carbon fibers degenerate the sphere-like. Substituting E_{a+m} into (15) and let the average microvoids volume fraction of thirty types carbon fibers replace f_2, we obtain the tensile modulus of amorphous carbon E_a, the value is 137.98 GPa.

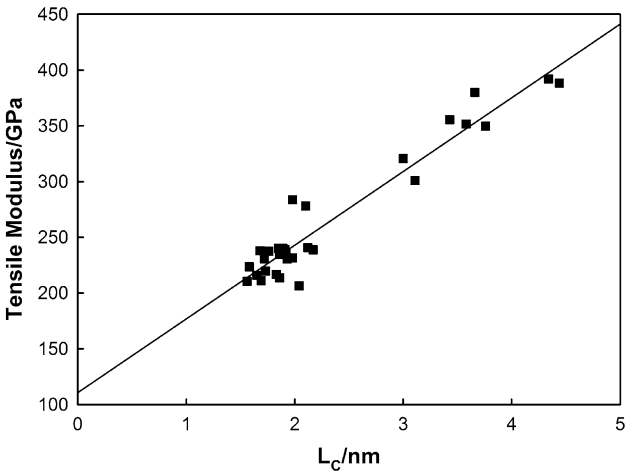

Fig. 2 Linear fiting plot of the data that reflect the relationship between the L_c and the tensile modulus for thirty different types of carbon fibers

SAXS

In order to obtain the radius of gyration R_g, the Guinier analysis is the most popular method in the SAXS analyses [22, 23]. According to Guinier theorem, we derive the expression of the intensity

$$I(h) = I^0 \exp\left(-\frac{h^2 R_g^2}{3}\right), \tag{20}$$

where $h = (4\pi \sin\theta)/\lambda$, λ is the wavelength of X-ray, 2θ is the scattering angle, and I^0 is the scattered intensity when $h = 0$. We can estimate the R_g value of the microvoids from the slope of the Guinier plot $\ln I(h)$ versus h^2. The Jellinek Successive tangents method is used here [24]. We divide the microvoids size into three classes according to the tangent line of the Guinier plot. We derive each class of the gyration radius R_{gi}, $i = 1, 2, 3$. The volume fraction of each class microvoids W_i, $i = 1, 2, 3$ and the average gyration radius $\overline{R_g}$ can be calculated respectively, by

$$W_i = \frac{K_i/R_{gi}^3}{\sum_i K_i/R_{gi}^3} \quad i = 1, 2, \tag{21}$$

$$\overline{R_g} = \sum_i R_{gi} W_i \quad i = 1, 2, 3, \tag{22}$$

where K_i is the intercept of the ith class tangent line in the vertical axis of the Guinier plot.

The radius of gyration at the direction of equator R_{gc} is independent of the length of rotation ellipsoids. Applying the formula $a = \sqrt{2}R_{gc}$, we can calculate the radial radius of the microvoids a. The difference of the microvoids in size is very small at the direction of equator [25], so we do not need to divide the radius of gyration at the direction of equator R_{gc} into three classes. We only divide the radius of gyration at the direction of meridian R_{gm}. Substitute a into the formula

$$R_{gmi} = \sqrt{\frac{a^2}{5} + \frac{L_i}{5}} \quad i = 1, 2, 3, \tag{23}$$

then $L = \sum_i W_i L_i \quad i = 1, 2, 3$. Detailed data are presented in Table 2.

The volume fraction of microvoids f_2 is given by the equation [26, 27]

$$f_2 = \frac{2\pi m^2 c^4}{e^4 \lambda^3 (\Delta\rho)^2 D t A I^0} \int_0^\infty I_a(h) h \, dh, \tag{24}$$

where $I_a(h)$ is the absolute X-ray intensity, which is determined by the direct method [28], $\Delta\rho$ is the electron density difference between the voids and the solid, m is the electron mass, c is the velocity of light, e is the elementary electric charge, D is the sample-to-detector distance, t is the specimen thickness, and AI^0 is the incident X-ray beam flux. See f_2 in Table 1.

Table 2 Experiment results of microvoids for the PAN-based carbon fibers

Type	Size of microvoids at the direction of equator		Size of microvoids at the direction of meridian				ω_v (L/a)
	R_{gc} (nm)	a (nm)	R_{gmi} (nm)	W_i (%)	L_i (nm)	L (nm)	
T300	1.04	1.48	1.97	98.07	3.88	4.02	2.72
			4.44	1.70	9.71		
			9.90	0.23	22.04		
T700	0.96	1.36	1.81	95.65	3.56	3.81	2.79
			3.79	3.24	8.26		
			6.80	0.91	15.07		
T800	0.97	1.38	2.09	94.37	4.25	4.82	3.33
			4.13	4.51	9.02		
			6.75	1.12	14.96		
M35J	1.03	1.46	1.97	95.73	3.90	4.16	2.85
			4.07	3.67	8.87		
			7.65	0.60	16.98		
M40J	0.99	1.40	2.16	95.44	4.40	4.67	3.34
			4.21	4.09	9.20		
			8.74	0.47	19.43		

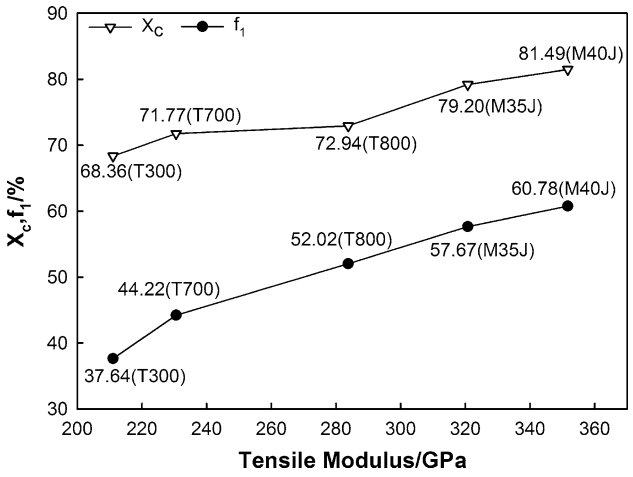

Fig. 3 Calculated volume fractions of crystallites

Calculated volume fractions of crystallites

To determine the volume fractions of crystallites of *T* series carbon fibers—T300, T700, and T800—and MJ series—M35J and M40J—the distribution density function of crystallites and microvoids must be first confirmed. In the case of carbon fibers with a high degree of crystallite orientation in the present study, the distribution density function $\eta_1(\theta)$ of the orientation angle θ between the normal of the carbon layer and the fiber axis can be closely approximated by an orientation distribution function of the form [29]

$$\eta_1(\theta) = K \sin^{\omega} \theta, \tag{25}$$

where

$$K = \frac{\Gamma[(\omega+3)/2]}{2\pi^{3/2}\Gamma[(\omega+2)/2]}$$

$$\omega = -\ln 2 / \ln[\sin(\pi\Pi/2)]$$

$\Gamma(x)$ is a gamma function having the following property $\Gamma(x+1) = x\Gamma(x)$ (real $x > 0$).

Assume that the rotation axis of crystallite is almost vertical to the rotation axis of microvoid. The orientation distribution function of microvoids is determined by the formula [30]

$$\eta_2(\theta) = \frac{\omega+1}{4\pi}|\cos\theta|^{\omega}, \tag{26}$$

where $\omega = -\ln 2/\ln[\sin(\pi\Pi/2)]$.

The volume fractions of crystallites of five samples can be calculated by substituting (25) and (26) into Eq. (15). See Fig. 3. The volume fractions of crystallites of five samples have a trend along the growth direction of tensile modulus. This trend is the same as the trend of apparent crystallinity.

Influence factors of tensile modulus

The orientation degree of crystallites Π, aspect ratios of crystallites ω_c, aspect ratios of microvoids ω_v, volume fractions of crystallites f_1, and volume fractions of microvoids f_2 are calculated by Eq. (15). Figure 4a (horizontal

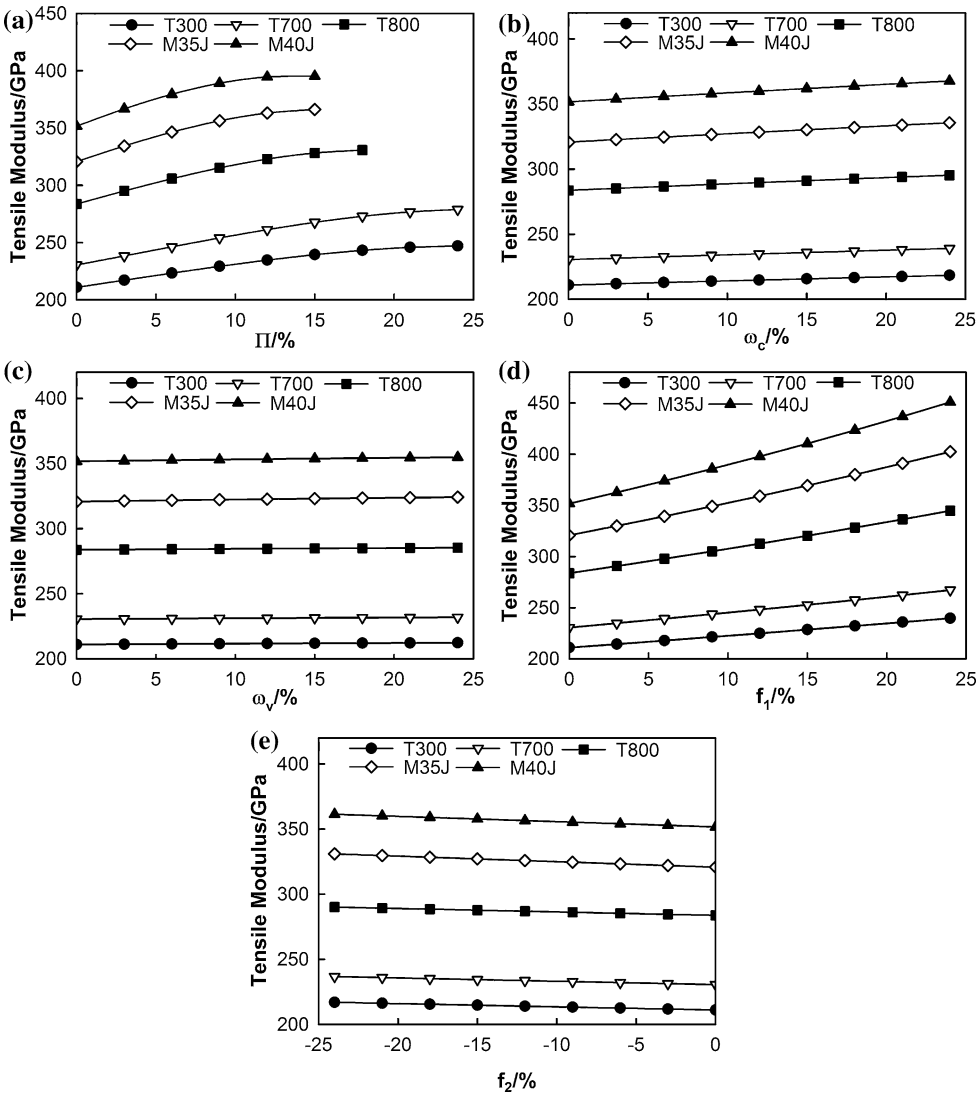

Fig. 4 Relationships between the tensile modulus and the factors for the bulk PAN-based carbon fibers

axis represents the increment of a factor, the same below) shows that the tensile modulus increases with increasing Π. The high modulus of a carbon fiber stems from the fact that the carbon layers, though not necessarily flat, tend to be parallel to the fiber axis [31]. The greater the degree of alignment of the carbon layers parallel to the fiber axis, the greater the fiber's tensile modulus. Comparing *T* series carbon fibers with MJ series carbon fibers, we can find that the MJ series have larger Π than the *T* series.' Five curves in Fig. 4a are different in length, because the five orientation degrees of crystallites had different initial values, which lie in the range 79–88 %, and the limit of orientation degree is 100 %. With Π close to 100 %, increases of tensile modulus gradually become slow. In Fig. 4b, the tensile modulus is plotted against ω_c. It can be seen that the tensile modulus increases linearly with ω_c in the interval $0\ \% \leq \omega_c \leq 24\ \%$. In a carbon fiber, there can be graphite regions of size L_c perpendicular to the carbon layers (crystallites) and size L_a parallel to the carbon layers. Both L_c and L_a grow with increasing heat treatment temperature in the processing of production of carbon fibers [20, 31, 32]; the greater the size of crystallites and ω_c, the greater the tensile modulus. We can find that the MJ series carbon fibers have larger size of crystallites and ω_c than the *T* series'. Figure 4c shows that the tensile modulus increases linearly with increasing ω_v, and five curves are almost horizontal lines. Elongated microvoids in carbon fibers along the fiber axis result in a high tensile modulus. On the contrary, dumpy microvoids can degrade the properties of carbon fibers. Figure 4d illustrates the tensile modulus plotted against the volume fractions of crystallites f_1. It is found that the tensile modulus shows a non-linear behavior with f_1. Usually, the greater the f_1, the higher the tensile modulus. Figure 4e shows that the tensile modulus increases linearly with descending f_2. It is obvious that the reduction of microvoids is good for the increase of the

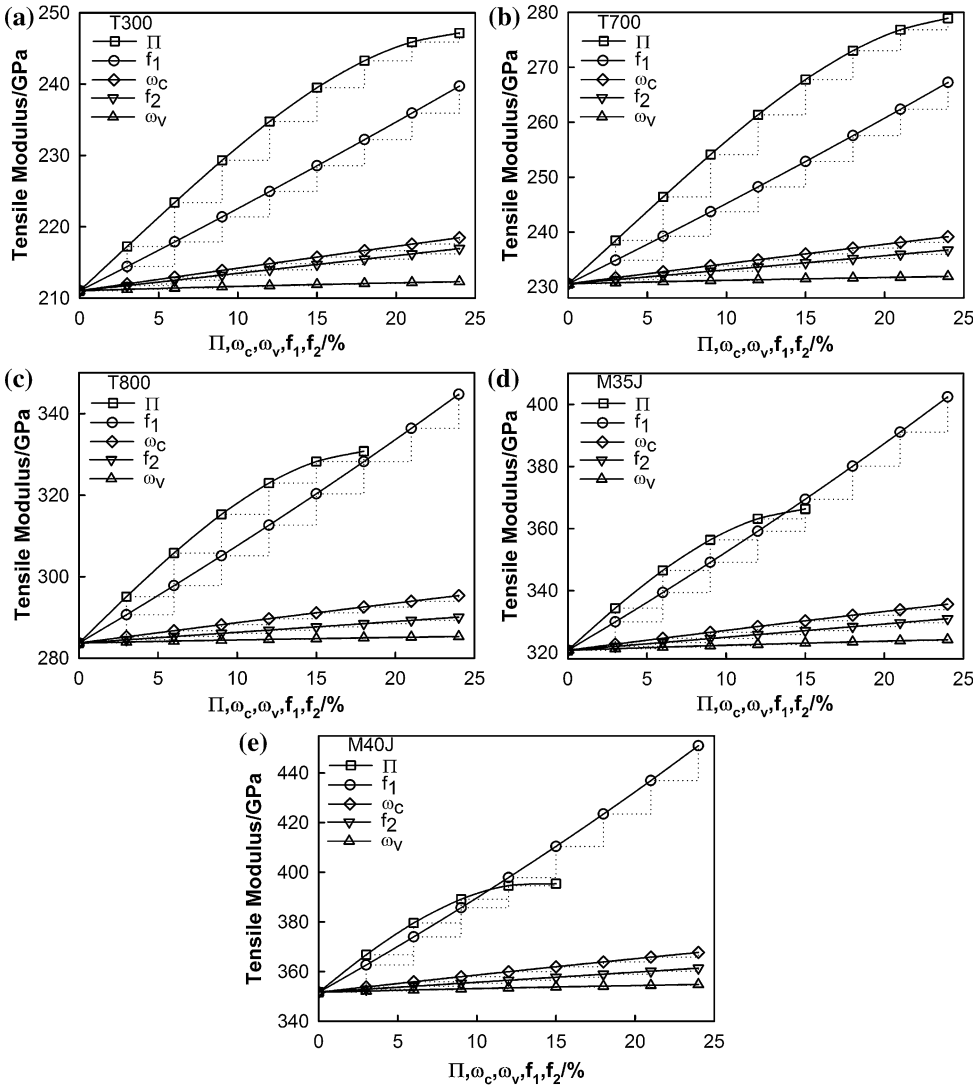

Fig. 5 Comparison between the factors for the bulk PAN-based carbon fibers

tensile modulus of carbon fibers, because the reduced volume of microvoids whose tensile modulus is zero transformed either crystallites or amorphous components or both of them.

Factors comparisons

The five factors Π, ω_c, ω_v, f_1, and f_2, which affect the tensile modulus of PAN-based carbon fibers, are discussed. Figure 5 shows the tensile modulus against the five factors for T300, T700, T800, M35 J, and M40 J (note that the curve of f_2 is in the second quadrant of the coordinate system, see Fig. 4e, we transform it into the first quadrant for comparison). In Fig. 5, we can see that ω_c, f_2, and ω_v have a smaller influence on the tensile modulus by considering the slope of curves. We can see that ω_c most affects the tensile modulus and f_2 is the next and ω_v is the last. Π and f_1 have a greater effect on tensile modulus than ω_c, f_2, and ω_v except for Π of M40J within the interval $12\ \% \leq \Pi \leq 15\ \%$, see Fig. 5e. Compare Π with f_1, and we can find that Π has a greater effect than f_1 in initial; with the increase of Π and f_1, the effect of Π on tensile modulus is surpassed by f_1 as shown Fig. 5a–e.

Conclusions

Our new three-phase micromechanical model which is established by applying the Eshelby equivalent inclusion theory and Mori–Tanaka's mean stress method can be successfully employed to predict the tensile modulus for carbon fibers. Using this micromechanical model, the volume fractions of crystallites of carbon fibers can be calculated which is able to apply to the quantitative calculation. It is noted that the present study has important implications for understanding the microstructural parameters that control the tensile modulus of

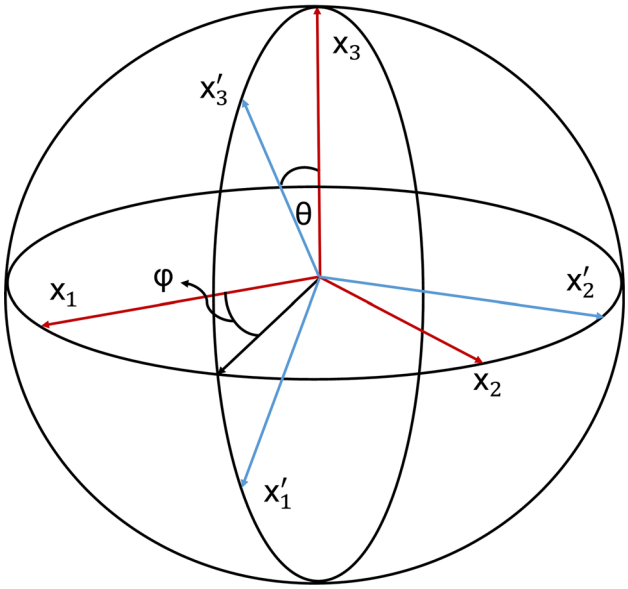

Fig. 6 Diagram of the global coordinate system and local coordinate system

PAN-based carbon fibers, such as the orientation degree of crystallites, volume fractions of crystallites and microvoids, and aspect ratios of crystallites and microvoids. By analyzing the new three-phase micromechanical model, we derive the tensile modulus of carbon fibers increase with increasing the orientation degree of crystallites, volume fractions of crystallites, aspect ratios of crystallites and microvoids, and the tensile modulus of carbon fibers increase with decreasing the volume fractions of microvoids. Comparing the five factors that influenced the tensile modulus of carbon fibers, we find that the volume fractions of crystallites and the aspect ratios of crystallites have the most significant effect for tensile modulus. The present study can provide useful help for improving mechanical properties and in the manufacturing process of carbon fibers.

Acknowledgements This work is supported by the National Natural Science Foundation of china (No. 11072069).

Appendix: coordinate transformation

Consider vector u in the global coordinate system $O - x_1x_2x_3$ and u' in the local coordinate system $O - x_1'x_2'x_3'$. See Fig. 6. The transformation relation between two coordinate systems can be expressed $u' = Qu$, where Q is a Transformation tensor. It can be written in matrix form as

$$Q = \begin{bmatrix} \cos\theta\cos\varphi & -\cos\theta\sin\varphi & \sin\theta \\ \sin\varphi & \cos\varphi & 0 \\ -\sin\theta\cos\varphi & \sin\theta\sin\varphi & \cos\theta \end{bmatrix}.$$

For second-order stress tensors σ in the global coordinate system and σ' in the local coordinate system, we have $\sigma = Q^T\sigma'Q$. Similarly, $\varepsilon = Q^T\varepsilon'Q$, where ε and ε' are second-order strain tensors in the global coordinate system and the local coordinate system, respectively.

Stress tensors and strain tensors can also be written in vectors form

$$\sigma = (\sigma_1\sigma_2\sigma_3\sigma_4\sigma_5\sigma_6)^T, \quad \varepsilon = (\varepsilon_1\varepsilon_2\varepsilon_3\varepsilon_4\varepsilon_5\varepsilon_6)^T$$

$$\sigma' \left(\sigma_1'\sigma_2'\sigma_3'\sigma_4'\sigma_5'\sigma_6'\right)^{\mathrm{T}} \varepsilon' = \left(\varepsilon_1'\varepsilon_2'\varepsilon_3'\varepsilon_4'\varepsilon_5'\varepsilon_6'\right)^{\mathrm{T}};$$

then the transformations of stress vectors and strain vectors are $\sigma = T\sigma'$ and $\varepsilon = (T^{-1})^{\mathrm{T}}\varepsilon'$, where T and $(T^{-1})^{\mathrm{T}}$ are the stress transformation matrix and strain transformation matrix, T^{-1} is inverse of the T, and $(T^{-1})^{\mathrm{T}}$ is transpose of the T^{-1}. T and $(T^{-1})^{\mathrm{T}}$ can be expressed as

$$T = \begin{bmatrix} T_A & 2T_B \\ T_C & T_D \end{bmatrix}, \quad (T^{-1})^{\mathrm{T}} = \begin{bmatrix} T_A & T_B \\ 2T_C & T_D \end{bmatrix},$$

where

$$T_{\mathrm{A}} = \begin{bmatrix} \cos^2\theta\cos^2\varphi & \sin^2\varphi & \sin^2\theta\cos^2\varphi \\ \cos^2\theta\sin^2\varphi & \cos^2\varphi & \sin^2\theta\sin^2\varphi \\ \sin^2\theta & 0 & \cos^2\theta \end{bmatrix},$$

$$T_{\mathrm{B}} = \begin{bmatrix} -\sin\theta\cos\varphi\sin\varphi & -\cos\theta\sin\theta\cos^2\varphi & \cos\theta\cos\varphi\sin\varphi \\ \sin\theta\cos\varphi\sin\varphi & -\cos\theta\sin\theta\sin^2\varphi & -\cos\theta\cos\varphi\sin\varphi \\ 0 & \cos\theta\sin\theta & 0 \end{bmatrix},$$

$$T_{\mathrm{C}} = \begin{bmatrix} -\cos\theta\sin\theta\sin\varphi & 0 & \cos\theta\sin\theta\sin\varphi \\ \cos\theta\sin\theta\cos\varphi & 0 & -\cos\theta\sin\theta\cos\varphi \\ -\cos^2\theta\cos\varphi\sin\varphi & \cos\varphi\sin\varphi & -\sin^2\theta\cos\varphi\sin\varphi \end{bmatrix},$$

$$T_{\mathrm{D}} = \begin{bmatrix} \cos\theta\cos\varphi & -\cos^2\theta\sin\varphi - \sin^2\theta\sin\varphi & \cos\varphi\sin\theta \\ \cos\theta\sin\varphi & \cos^2\theta\cos\varphi - \sin^2\theta\cos\varphi & \sin\theta\sin\varphi \\ -\cos^2\varphi\sin\theta + \sin\theta\sin^2\varphi & 2\cos\theta\sin\theta\cos\varphi\sin\varphi & \cos\theta\cos^2\varphi - \cos\theta\sin^2\varphi \end{bmatrix}.$$

References

1. Oberlin A (1984) Carbonization and graphitization. Carbon 22(6):521–541
2. Johnson DJ (1987) Structure-property relationships in carbon fibers. J Phys D Appl Phys 20(3):286–291
3. Johnson DJ (1987) Structural studies of PAN-based carbon fibers. In: Thrower PA (ed) Chemistry and physics of carbon, vol 20. Marcel Dekker, New York, pp 1–58
4. Oberlin A, Bonnamy S, Lafdi K (1989) Structure and texture of carbon fibers. In: Donnet JB (ed) Carbon fibers. Mercel Dekker Inc, New York, pp 85–159
5. Ruland W (1969) The relationship between preferred orientation and Young' s modulus of carbon fibers. Appl Polym Symp 9:293–301
6. Northolt MG, Veldhuizen LH, Jansen H (1991) T ensile deformation of carbon fibers and the relationship with the modulus for shear between the basal planes. Carbon 29(8):1267–1279
7. Shioya M, Hayakawa E, Takaku A (1996) Non-hookean stress-strain response and changes in crystallite orientation of carbon fibers. J Mater Sci 31(17):4521–4532. doi:10.1007/BF00366347
8. Morita K, Murata Y, Ishitani A, Murayaya K, Ono T, Nakajima A (1986) Characterization of commercially-available PAN (polyacrylonitrile)-based carbon fibers. Pure Appl Chem 58:455–468
9. Kobayashi T, Sumiya K, Fujii Y, Fujie M, Takahagi T, Tashiro K (2012) Stress-induced microstructural changes and crystallite modulus of carbon fiber as measured by X-ray scattering. Carbon 50:1163–1169
10. Tanaka F, Okabe T, Okuda H, Ise M, Kinloch IA, Mori T et al (2013) The effect of nanostructure upon the deformation micromechanics of carbon fibers. Carbon 52:372–378
11. Andreas AF, Ruland W (2000) Microvoids in Polyacrylonitrile Fibers: a Small-Angle X-ray Scattering Study [J]. Macromolecules 33:1848–1852
12. Eshelby JD (1957) The determination of the elastic field of an ellipsoidal inclusion, and related problems. Proc R Soc A 241(1226):376–396
13. Eshelby JD (1959) The elastic field outside an ellipsoidal inclusion. Proc R Soc A 252(1271):561–569
14. Mori T, Tanaka K (1973) Average stress in matrix and average elastic energy of materials with misfitting inclusions. Acta Met 21(5):571–574
15. Li Shaofan, Wang Gang (2008) Introduction to micrmechanics and nanomechanics. World Scientific, Singapore
16. Dvorak George J (2013) Micromechanics of composite materials. Springer, London
17. Spence GB (1963) Extended dislocation in the anisotropic elastic continuum approximation. Proceedings of the fifth conference on carbon. American Carbon Society, Pennsylvania, pp 531–538
18. Qiu YP, Weng GJ (1990) On the application of Mori-Tanaka's theory involving transversely isotropic spheroidal inclusions. Int Eng Sci 28:1121–1137
19. Mura T (1987) Micromechanics of defects in solids. Martinus Nijhoff, The Netherlands
20. He F (2004) Carbon Fiber and Applied Technique [M]. Chemical Industry Press, Beijing
21. Liu FJ, Wang HJ, Fan LD (2009) Analysis on the microstructure of MJ series carbon fibers. New Chem Mater 37(1):41–43
22. Zhu YP (2008) Small angle X-ray scattering-theory, measurement, calculation and application. Chemical Industry Press, Beijing
23. Fukuyama Katsuya, Kasahara Yasutoshi, Kasahara Naoto, Oya Asao et al (2001) Small-angle X-ray scattering study of the pore structure of carbon fibers prepared from a polymer blend of phenolic resin and polystyrene. Carbon 39:287–324
24. Yin JH, Mo ZS (2001) Modern Polymer Physics [M]. Science-Press, Beijing
25. Sheng Y, Zhang CH, Xu Y et al (2009) Investigation of PAN-based carbon fiber microstructure by 2D-SAXS. New Carbon Mater 24(3):270–276
26. Shioya M, Takaku A (1985) Characterization of microvoids in carbon fibers by absolute small angle X-ray measurements on a fiber bundle. J Appl Phys 58:4074–4082
27. Shioya M, Takaku A (1986) Characterization of microvoids in polycrylonitrile based carbon fibers. J Mater Sci 21:4443–4450. doi:10.1007/BF01106569
28. Weinberg DL (1963) Absolute intensity measurements in small angle X-ray scattering. Rev Sci Instrum 34(6):691–696
29. Shioya M, Takaku A (1994) Rotation and extension of crystallites in carbon fibers by tensile stress. Carbon 32:615–619
30. Mao YM (2011) Polymorphism, preferred orientation and morphology of propylene-based random copolymer subjected to external force fields. PhD Dissertation, Stony Brook University
31. Deborah DDL (1994) Carbon fiber composites. Butterworth-Heinemann, Boston
32. Su CJ, Gao AJ, Lu S, Xu LH (2012) Evolution of the skin-core structure of PAN-based carbon fibers with high temperature treatment. New Carbon Mater 27:288–293 **[in Chinese]**